ELSEVIER

Journal of Molecular Catalysis A: Chemical 149 (1999) 263–273

JOURNAL OF MOLECULAR CATALYSIS A: CHEMICAL

www.elsevier.com/locate/molcata

TAP study of the sorption of H_2 and O_2 on $Rh/\gamma\text{-}Al_2O_3$

Olivier Dewaele [1], Dezheng Wang [2], Gilbert F. Froment *

Laboratorium voor Petrochemische Techniek, Universiteit Gent, Krijgslaan 281 S5, B9000 Gent, Belgium

Received 27 November 1998; received in revised form 14 January 1999; accepted 8 March 1999

Abstract

The sorption kinetics on $Rh/\gamma\text{-}Al_2O_3$ with a very low Rh loading of hydrogen between 523 and 673 K and of oxygen between 773 and 1073 K were determined by means of a TAP reactor. The adsorption and desorption rates of hydrogen and oxygen show a second-order dependence in the concentration of free sites and the concentration of occupied sites, respectively. The desorption activation energy amounts to 57 kJ mol^{-1} for hydrogen desorption and 140 kJ mol^{-1} for oxygen desorption. The sorption model for oxygen involves reversible exchange of adsorbed oxygen between two adsorption states on the surface.

Keywords: Temporal analysis of products; Rh; $\gamma\text{-}Al_2O_3$; Oxygen; Hydrogen; Kinetics

1. Introduction

Rh is a catalyst for several interesting industrial reactions such as oxidation [1], reforming [2] and (de)hydrogenation [3,4]. For these reactions, the knowledge of the sorption kinetics of hydrogen and oxygen on Rh is important as evidenced by a number of studies devoted to the determination of these kinetics on unsupported Rh [5–18].

Literature data on the sorption of hydrogen on unsupported Rh are very much in agreement. The adsorption rate of hydrogen is proportional to the square of the concentration of free adsorption sites and is not activated [5,6]. The desorption rate of hydrogen is shown to be proportional to the square of the concentration of adsorbed hydrogen. The activation energy for desorption is in the range 80 to 100 kJ mol^{-1} [5–8,14,15]. Experimental data indicating the presence of a hydrogen desorption precursor were also published [5–7,14,15]. The interaction of oxygen with unsupported Rh is less well understood. The adsorption rate of oxygen shows a first-order dependence in the number of Rh sites at temperatures around 333 K [5], but it is assumed to follow nonactivated second-order kinetics at higher temperatures [16,17]. Temperature programmed desorption of oxygen from different Rh faces reveals several peak temperatures, indicating the existence of different adsorption states [9–12,18]. The reported activation energy for oxygen desorption varies be-

* Corresponding author. Department of Chemical Engineering, Texas A&M University, College Station, TX 77843-3122, USA. E-mail: gilbert.froment@skynet.be

[1] Present address: UOP R&D, Engineering Science Skill Center, 25 East Algonquin Road, Des Plaines, IL 60017-5017, USA.

[2] Present address: State Key Laboratory of Catalysis, Dalian Institute of Catalysis, Chinese Academy of Sciences, PO Box 110, Dalian, 116023, China.

1381-1169/99/$ - see front matter
PII: S1381-1169(99)00189-2

tween 120 and 360 kJ mol^{-1}, depending on the surface coverage [10–13,18]. Dissolution into the bulk has also been suggested [11–13]. The formation of a second oxygen adsorption state or a surface oxide at higher temperatures [8,16,19,20] and the existence of repulsive oxygen interactions on the surface [11,13] have been reported. The reconstruction of the Rh surface upon oxygen adsorption is presently being studied [21,22].

Very little information is available on the sorption kinetics of oxygen and hydrogen on supported Rh [23–25]. This is especially the case for catalysts with a very low Rh loading. Therefore, the aim of this study is to present an appropriate experimental technique to determine the kinetics for the sorption of hydrogen and oxygen on supported Rh at higher temperatures. Moreover, many catalytic reactions proceed on a time scale that is too large to be studied with the TAP reactor by means of the conventional pulse experiments and data treatment. In this study, it is shown how quantitative information can be obtained in these cases for the reversible adsorption and desorption. The same procedure can be applied for complex reactions.

2. Experimental procedure

The experiments were performed in a TAP reactor system from Autoclave Engineers. The TAP system has been described in detail previously [26]. Essentially, the apparatus is used as a pulse reactor operating under vacuum, i.e., at 10^{-4} to 10^{-5} Pa background pressure. Small amounts of reactant are injected into a tubular reactor. Although the pulse size can be varied between 10^{13} and 10^{17} molecules, it was chosen below 5×10^{15} molecules to ensure that the transport mechanism in the reactor is of the Knudsen diffusion type. The injection time is less than 1 ms. The reactor is a quartz reactor, 35 mm long and 5 mm in diameter. The product fluxes at the outlet of the reactor are measured by means of a UTI-100C quadrupole mass spectrometer with a time resolution of less than 0.1 ms.

The $Rh/\gamma\text{-}Al_2O_3$ catalyst has a Rh loading of 0.05 wt.% and was prepared by incipient wetness impregnation with $RhCl_3 \cdot H_2O$. The catalyst was dried at 373 K and calcined at 523 K, followed by reduction at 473 K for 20 min. The BET surface was 153 $m^2\ g^{-1}$. The average pore diameter was 5.3 nm. The catalyst bed was diluted with quartz particles and placed between two quartz beds at the inlet and outlet of the reactor. The particle size was between 250 and 500 μm. Prior to all experiments, the catalyst was dehydroxylated under vacuum at 1073 K. The purity of the O_2, H_2, Ar and He feeds exceeded 99.9%.

The hydrogen pulse responses were obtained by injecting a H_2/He mixture at different pulse sizes over 0.12 g of reduced and dehydroxylated catalyst. The bed consisted of 7 mm quartz packing at the inlet, 10 mm quartz/catalyst mixture in the center and 15 mm quartz packing at the outlet of the reactor. The pulse frequency was 1 pulse per 1.054 s. The tail of the hydrogen responses exceeded 1.054 s. Therefore, many preliminary pulses were needed to ensure that the collected pulse response was independent of the pulse number. Thirty pulse responses were collected and were averaged for noise reduction. The hydrogen background signal was measured after each experiment and a mass balance with He was calculated to verify that no hydrogen was irreversibly adsorbed.

The oxygen responses were obtained in the same manner as those of hydrogen by means of single pulse experiments with an O_2/Ar mixture with 0.12 g of catalyst. The reactor consisted of 8 mm quartz packing at the inlet, 10 mm quartz/catalyst mixture in the center and 12 mm quartz packing at the outlet of the reactor. Before each experiment, hydrogen was injected and the catalyst was dehydroxylated to ensure that the surface was metallic Rh and not Rh_2O_3. The formation of the latter was seen as a decrease of the interaction of O_2 with the catalyst when no pre-reduction was applied.

3. Experimental results

3.1. Interaction of hydrogen with the catalyst

The normalized periodic hydrogen responses to a hydrogen pulse train for different pulse sizes at 573 and 673 K and the normalized helium response to helium pulses at 573 K are shown in Fig. 1. A pulse size dependence which becomes less pronounced at higher temperatures is evident (Fig. 1). Larger pulses result in narrower pulse responses (Fig. 1). This can be caused by site saturation or by a second-order dependence of the hydrogen desorption rate with respect to the concentration of adsorbed hydrogen. Site saturation would cause a higher mean coverage with larger pulse sizes resulting in less interaction of hydrogen with the catalyst and sharper responses. The second-order dependence would also give sharper responses with

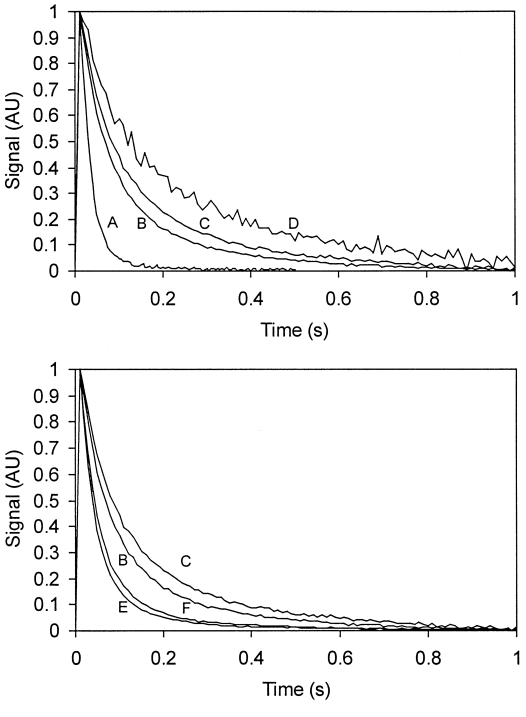

Fig. 1. Hydrogen responses to hydrogen pulses with different pulse sizes at 573 and 673 K. (A) He; (B and E) H_2 1.8×10^{15} molecules per pulse. (C and F) H_2 1.2×10^{15} molecules per pulse. (D) H_2 4.2×10^{14} molecules per pulse. (A, B, C and D) 573 K; (E and F) 673 K.

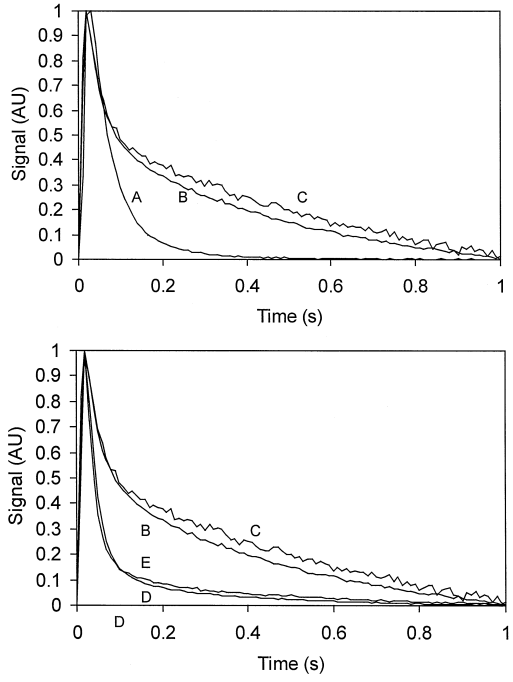

Fig. 2. Oxygen responses to oxygen pulses with different pulse sizes at 923 and 823 K. (A) Ar; (B and D) 1.4×10^{15} molecules per pulse; (C and E) 6.9×10^{14} molecules per pulse. (A, B and C) 923 K; (D and E) 823 K.

larger pulse sizes because of the smaller mean life time of hydrogen on the surface due to the higher coverage. The response width decreases with increasing temperature as a result of the higher desorption rate at higher temperatures. The pulse size was very small compared to the amount of Rh in the reactor and no large tail in the hydrogen responses was seen above 573 K. Therefore, it can be assumed that the hydrogen coverage was low during the experiments and that no site saturation occurs. The second-order dependence of the desorption rate in adsorbed hydrogen is the more probable cause of the broadening of the responses.

3.2. Interaction of oxygen with the catalyst

The periodic oxygen responses show a behavior which is different from that of hydrogen (Fig. 2). There is also a pulse size dependence,

but this dependence and the response width increase with temperature (Fig. 2). This proves that the oxygen coverage of the Rh was high during the measurement of the oxygen responses since the lower coverage at higher temperatures significantly increases readsorption. The part of the oxygen response between 0 and 0.2 s at 923 K does not change with the pulse size. This part, however, broadens at higher temperatures, indicating that this peak does not result from nonadsorbed oxygen. It was impossible to identify the cause of the pulse size dependence of the oxygen responses since the experiments were performed at a higher oxygen coverage.

4. Modeling of the pulse responses

4.1. Reactor model

The reactor is packed at the inlet with an inert bed with length L_i (m_r). The catalyst bed, having a length L_c (m_r), is placed in the center of the reactor. It is followed by an inert bed with length L_e (m_r). The continuity equations for the gas phase Eq. (1) and surface components Eq. (2) are written:

$$\frac{\partial}{\partial z}\left(D_i\frac{\partial C_g}{\partial z}\right)=\varepsilon_i\frac{\partial C_g}{\partial t} \qquad 0<z<L_i,$$

$$\frac{\partial}{\partial z}\left(D_c\frac{\partial C_g}{\partial z}\right)+\rho_B R_{v,g}=\varepsilon_c\frac{\partial C_g}{\partial t} \qquad L_i<z<L_i+L_c, \tag{1}$$

$$\frac{\partial}{\partial z}\left(D_i\frac{\partial C_g}{\partial z}\right)=\varepsilon_i\frac{\partial C_g}{\partial t} \qquad L_i+L_c<z<L_i+L_c+L_e,$$

$$\frac{\partial C_s}{\partial t}=R_{v,s} \qquad L_i<z<L_i+L_c, \tag{2}$$

with C_g (mol m_g^{-3}) the gas phase concentration, C_s (mol kg_c^{-1}) the concentration surface components, D_c and D_i (m_g^3 m_r^{-1} s^{-1}) the Knudsen diffusivities in the catalyst and inert bed, $R_{v,g}$ and $R_{v,s}$ (mol kg_c^{-1} s^{-1}) the formation rates of the gas phase and surface components, t (s) time, z (m_r) the axial position in the reactor, ε_c and ε_i (m_g^3 m_r^{-3}) the void fractions of the catalyst and inert bed, and ρ_B (kg_c m_r^{-3}) the bulk density of the catalyst bed.

The quartz reactor has an important inlet volume V_0 (m_r^3). The concentrations in this inlet volume are equal to those at the inlet of the reactor bed. Once filled, the time variation of the concentration of a component of the pulse is uniform over the complete inlet volume. The boundary condition for the inlet of the reactor bed is obtained from a mass balance over the inlet volume and an incremental distance dz inside the reactor bed:

$$V_0\left(\frac{\partial C_g}{\partial t}\right)_v-F_{in}=SD_i\left(\frac{\partial C_g}{\partial z}\right)_{z=0}, \tag{3}$$

with F_{in} (mol s^{-1}) the flux at the inlet of the reactor and S (m_r^2) the cross-section of the reactor.

The boundary conditions between the beds express that the concentration profiles and the flux profiles are continuous functions of z:

$$\begin{aligned}
&(C_g)_{z=L_i-}=(C_g)_{z=L_i+},\\
&\left(D_i\frac{\partial C_g}{\partial z}\right)_{z=L_i-}=\left(D_c\frac{\partial C_g}{\partial z}\right)_{z=L_i+},\\
&(C_g)_{z=(L_i+L_c)-}=(C_g)_{z=(L_i+L_c)+},\\
&\left(D_c\frac{\partial C_g}{\partial z}\right)_{z=(L_i+L_c)-}=\left(D_i\frac{\partial C_g}{\partial z}\right)_{z=(L_i+L_c)+}.
\end{aligned} \tag{4}$$

The rate at which molecules are leaving the reactor towards the mass spectrometer is equal to the rate at which they are transported in the bed by Knudsen diffusion towards the exit of the reactor. Zou et al. [27] studied this boundary condition and came to the conclusion that approximating the concentration at the exit of the reactor by zero is an equivalent boundary condition if $D_i\,u^{-1}\,\varepsilon_i^{-1}\,L_{tot}^{-1}$ is very small. The latter

condition was fulfilled in the present study. The following exit boundary condition was used:

$$\left(C_g\right)_{z=L_{tot}} = -\left(\frac{D_i}{u\varepsilon_i}\frac{\partial C_g}{\partial z}\right)_{z=L_{tot}} \approx 0, \qquad (5)$$

with L_{tot} (m_r) the length of the reactor packing and u ($m_r\ s^{-1}$) the mean velocity of the gas phase molecules.

Finally, the response I can be expressed as the flux leaving the reactor at the exit of the reactor:

$$I = -SD_i\left(\frac{\partial C_g}{\partial z}\right)_{z=L_{tot}}. \qquad (6)$$

The pulse responses that have to be simulated, are the periodic responses to a single pulse experiment with a large number of pre-measurement pulses. The broadening of the oxygen and hydrogen responses is too large to allow the tail of the responses to reach the base line. The initial conditions for these cases are the concentration profiles at the end of the preceding pulse response. Determination of these initial conditions is not straight forward. The most logical way would consist of simulating the large pulse train iteratively, starting with zero initial concentrations. The amount of iterations to obtain a periodic pulse response can be very large, depending on the pulse size and the amount of active sites.

The following method can be applied to reduce the number of iterations. Instead of using gas phase and surface concentrations equal to zero as the initial conditions, concentration profiles during steady state operation of the reactor are used as initial values. The continuous feed rate is equal to the pulse size N_0 (mol) divided by the pulse period Δt (s). For the case where only adsorption and desorption occur the initial gas phase concentration profiles can be calculated from:

$$\frac{\partial C_g}{\partial z} = -\frac{N_0}{\Delta t SD_{i\,or\,c}} \qquad 0 < z < L_i + L_c + L_e,$$

$$C_g = 0 \qquad z = L_i + L_c + L_e. \qquad (7)$$

In this study, the initial gas phase concentration profiles were approximated by means of Eq. (8):

$$\left(C_g\right)_{t=0} = \frac{N_0}{\Delta t SD_{i\,or\,c}}\left(L_i + L_c + L_e - z\right). \qquad (8)$$

The number of iterations can also be reduced by the following procedure. After the three first iterations or after two consecutive iterations, a new set of initial concentration profiles C^{new} is calculated by means of the following equation:

$$C^{new} = \mathrm{MAX}\left(\frac{C^i - C^{i-1}}{C^{i-1} - C^{i-2}}, 0\right)\left(C^i - C^{i-1}\right) + C^i, \qquad (9)$$

in which C^i is the concentration profile obtained from the last iteration, C^{i-1} is the initial concentration profile used for the last iteration and C^{i-2} is the initial concentration profile used for the second last iteration. The use of the maximum (MAX) allows a stable evolution of the iteratively calculated responses. Fig. 3 shows the efficiency of the methods described above in decreasing the number of iterations. Both methods reduce the number of iterations by at least a factor of 2.

The Bulirsch–Stoer numerical integration routine with finite differentiation throughout the reactor was applied to solve the set of differen-

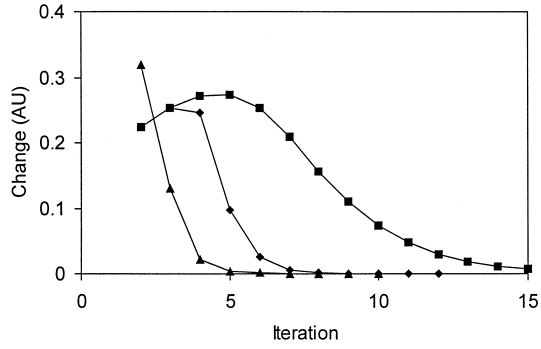

Fig. 3. Relative variation of the pulse responses as a function of the number of iterations. (■) Initial concentration profile equal to zero; (♦) With extrapolation by means of Eq. (9). (▲) With extrapolation Eq. (9) and calculation from the steady state operation Eq. (8).

tial equations. The kinetic parameters were estimated by means of the Rosenbrock and the Levenberg–Marquardt algorithm. The iterative calculation of the periodic pulse response was discontinued when the relative change of the calculated responses, defined as the sum of the absolute change of the different calculated data points, was lower than 10^{-4}. The temperature profiles in the reactor were taken into account.

4.2. Hydrogen responses

The hydrogen responses were simulated by means of the reactor model described in the previous paragraph. The Knudsen diffusivities of hydrogen were calculated from the estimated helium diffusivities and the ratio of the diffusivity of hydrogen to that of helium. The latter was obtained by estimating both diffusivities from hydrogen and helium responses in an inert quartz bed. Molecular sorption with a first-order dependence of the adsorption and desorption rates with respect to the hydrogen gas phase concentration and the surface concentration resulted in a poor fit of the pulse responses. A reaction scheme with dissociative adsorption and recombinative desorption resulted in a good fit (Fig. 4). This scheme and the corresponding equations for the adsorption rate r_a (mol kg_c^{-1} s^{-1}) and the desorption rate r_d (mol kg_c^{-1} s^{-1}), are shown below:

$$H_2 + 2l \rightarrow 2H - l \quad r_a = \varepsilon_c k_a C_{H_2}(1-\theta_H)^2, \tag{10}$$

$$2H - l \rightarrow H_2 + 2l \quad r_d = k_d \theta_H^2, \tag{11}$$

with l an active site, k_a (m_r^3 kg_c^{-1} s^{-1}) the adsorption rate coefficient, k_d (mol kg_c^{-1} s^{-1}) the desorption rate coefficient, C_{H_2} (mol m_g^{-3}) the gas phase concentration of hydrogen, and θ_H the fraction of the surface cover with adsorbed hydrogen.

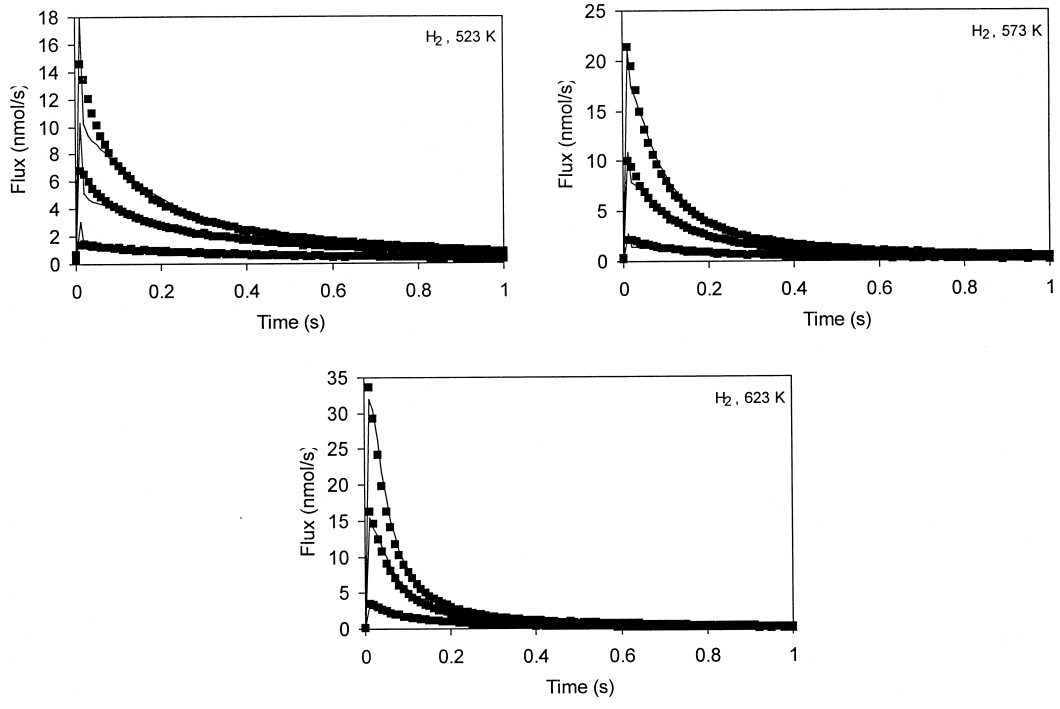

Fig. 4. Experimental and simulated hydrogen responses obtained with 0.12 g of catalyst.

Table 1
Parameter estimates and 95% confidence intervals for the sorption model of hydrogen

Parameter	Estimated value
C_t (10^{-4} mol kg_c^{-1})	4.74 ± 1.25
k_a (m_r^3 kg_c^{-1} s^{-1})	1.58 ± 1.06
k_d (mol kg_c^{-1} s^{-1}), 573 K	0.159 ± 0.06
E_d (kJ mol^{-1})	56.60 ± 1.33

At 523 K, the model does not fit the responses well between 0 and 0.05 s. The reason for this small deviation is not clear. It could be caused by hydrogen spillover or by a molecular sorption precursor [5–7,14,28]. It was assumed that the adsorption is not activated. Only the desorption activation energy E_d (kJ mol^{-1}), the adsorption and desorption rate coefficients k_a (m_r^3 kg_c^{-1} s^{-1}) and k_d (mol kg_c^{-1} s^{-1}), and the concentration of sorption sites C_t (mol kg_c^{-1}) were estimated. Table 1 contains the estimated parameters and their 95% confidence intervals.

4.3. Oxygen responses

The oxygen responses were simulated and kinetic parameters were determined as described above. The Knudsen diffusivities of oxygen in the beds were calculated by multiplying the diffusivity of argon, estimated from the argon responses, with the square root of the ratio of the argon to the oxygen molecular weight. Molecular sorption and dissociative sorption were not able to describe the observed responses. As mentioned in paragraph 3, two active sites or two sorption states of oxygen are expected to be present on the surface. Different reaction schemes were tested. The scheme that yielded the best fit is shown in Eqs. (12)–(15). The corresponding reaction rates are also presented. The scheme consists of reversible dissociative adsorption of oxygen and transformation of the adsorbed oxygen $(O-l)$ to a second adsorption state (O^*-l). C_{O_2} (mol m_g^{-3}) is the gas phase concentration oxygen, θ_O and θ_{O^*}

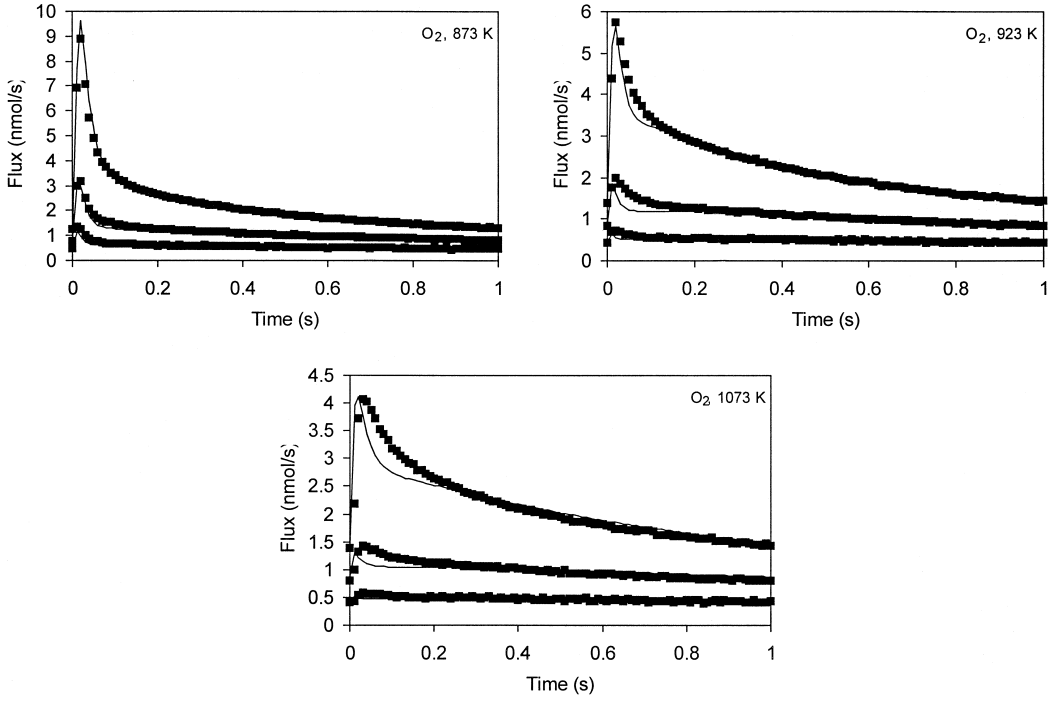

Fig. 5. Experimental and simulated oxygen responses obtained with 0.12 g of catalyst.

Table 2
Parameter estimates and 95% confidence intervals for the sorption model of oxygen

Parameter	Estimated value
C_t (10^{-4} mol kg_c^{-1})	3.12 ± 0.12
k_a (m_r^3 kg_c^{-1} s^{-1})	13.1 ± 0.73
k_d (10^{-3} mol kg_c^{-1} s^{-1}), 1073 K	5.55 ± 0.41
k_{12} (10^{-5} mol kg_c^{-1} s^{-1}), 1073 K	2.89 ± 0.12
k_{21} (10^{-5} mol kg_c^{-1} s^{-1}), 1073 K	1.10 ± 0.06
E_d (kJ mol^{-1})	139.6 ± 1.0
E_{12} (kJ mol^{-1})	272.1 ± 8.8
E_{21} (kJ mol^{-1})	151.7 ± 6.5

are the surface coverage of chemisorbed oxygen, r_{12}, r_{21}, k_{12} and k_{21} (mol kg_c^{-1} s^{-1}) are the exchange rates and exchange rate coefficients between the adsorbed oxygen species.

$$O_2 + 2l \rightarrow 2O - l$$

$$r_a = \varepsilon_c k_a C_{O_2}(1 - \theta_O - \theta_{O^*})^2, \quad (12)$$

$$2O - l \rightarrow O_2 + 2l \quad r_d = k_d \theta_O^2, \quad (13)$$

$$O - l \rightarrow O^* - l \quad r_{12} = k_{12} \theta_O, \quad (14)$$

$$O^* - l \rightarrow O - l \quad r_{21} = k_{21} \theta_{O^*}. \quad (15)$$

The fit between the experimental and the simulated responses are shown in Fig. 5. Table 2 shows the estimates of the kinetic parameters. The adsorption rate is assumed not activated.

4.4. Sticking probabilities

The sticking probabilities of H_2 and O_2 were calculated from the estimated value of k_a (m_r^3 kg_c^{-1} s^{-1}). The following equation is the basis for this calculation:

$$s_o q Z = \varepsilon_c k_a \rho_B C_g. \quad (16)$$

This equation expresses that the collision frequency Z (mol m_r^{-3} s^{-1}) multiplied by the sticking probability s_o on an active site and the fraction q of the surface in the reactor taken by the active phase, equals the consumption rate of oxygen per cubic meter reactor. The collision frequency Z per cubic meter reactor will be calculated from the mean velocity u (m_r s^{-1}) of the gas phase molecules and the mean free path Λ (m_r) in the catalyst bed:

$$Z = \varepsilon_c \frac{u}{\Lambda} C_g. \quad (17)$$

The mean velocity u and the mean free path Λ can be calculated from:

$$u = \sqrt{\frac{8RT}{\pi M}}, \quad (18)$$

$$\Lambda = 3\frac{D_c}{u\varepsilon_c}, \quad (19)$$

with M the molecular weight (kg mol^{-1}), R the universal gas constant (J mol^{-1} K^{-1}), and T the temperature (K).

The above equations lead to the following expression for the sticking probability s_o:

$$s_o = \frac{3D_c k_a \rho_B}{q\varepsilon_c u^2}, \quad (20)$$

or:

$$s_o = \frac{3D_c k_a \rho_B \pi M}{8 q \varepsilon_c RT}. \quad (21)$$

Table 3 presents the sticking probability of oxygen and hydrogen on the active sites and the values of the properties entering in their calculation. The sticking probability of hydrogen is about 0.05, that of oxygen is estimated to be about 2, which, obviously is too large.

Table 3
Sticking probabilities of oxygen and hydrogen on the active sites and the values of the properties involved in their calculation

	Hydrogen	Oxygen
T_r (K)	573.15	1023.15
u (m_r s^{-1}), at T_r	2453.8	822.80
D_c / ε_c (m_r^2 s^{-1})	0.01545	0.005284
C_t (10^{-4} mol kg_c^{-1})	4.74 ± 1.25	3.12 ± 0.12
q (10^{-4})	1.40 ± 0.37	0.923 ± 0.035
Λ (m_r)	1.89×10^{-5}	1.92×10^{-5}
k_a (m_r^3 kg_c^{-1} s^{-1})	1.58 ± 1.05	13.1 ± 0.73
ρ_B (kg_c m_r^{-3})	610.4	766.2
s, at T_r	0.053 ± 0.037	2.55 ± 0.18

Rh: 2.21×10^{-5} mol m^{-2}.

5. Discussion

The observed hydrogen pulse responses were fairly accurately simulated by means of a model involving dissociative adsorption of hydrogen. Based on literature data, the adsorption of hydrogen was assumed not activated [5–8]. The activation energy for hydrogen desorption was estimated to be 56.6 kJ mol^{-1}. An activation energy of about 80 to 100 kJ mol^{-1} is reported in the literature for the desorption of hydrogen from unsupported Rh catalysts [5–8,14,15]. The number of sorption sites was found to be 4.74 $\times 10^{-4}$ mol kg_c^{-1}. From this value, a dispersion of the Rh on the catalyst of about 9.7% can be calculated. This corresponds very well with the value of 9.8% obtained during titration of the Rh catalyst at room temperature by means of hydrogen and oxygen pulse chemisorption. The sticking probability of hydrogen on the supported Rh catalyst was estimated to be 0.053. TPD spectra of hydrogen at different initial coverages were simulated by means of the hydrogen sorption model. A peak temperature of 353 K was found for the TPD spectrum with initial full coverage (Fig. 6). At lower initial surface coverage, a higher peak temperature is obtained. The results presented above are in agreement with literature data [9,15].

The reaction scheme for the sorption of oxygen, consisting of dissociative oxygen adsorption and exchange of adsorbed oxygen between two sorption states, leads to a good fit of the responses. This scheme is in agreement with the scheme presented by Zum Mallen et al. [16] from their study of the oxidation of hydrogen with oxygen on Rh, and with the observations of Oh and Carpenter [29] and Kim et al. [30], who detected the formation of a surface oxide during the oxidation of CO. The estimated concentration of active sites corresponds very well with that derived from the hydrogen responses and with the value obtained from pulse chemisorption at room temperature. Another scheme which resulted in an equally good fit of the responses is a scheme consisting of reversible dissociative adsorption of oxygen and exchange of adsorbed oxygen between a second sorption site. This lead however to an estimated number of active sites which was too low. Calculation of the sticking probability of oxygen yields a value of 2.5. This is obviously too large. In the present work, the adsorption rate coefficient was considered to be independent of the temperature which could explain the deviation. Simulation of the TPD spectra of oxygen at various initial coverages using the estimated kinetic parameters, yields a peak temperature of 813 K at full initial coverage (Fig. 5). Peak temperatures between 773 and 1073 K are reported in the literature [9–12,18]. The activation energy for oxygen desorption was found to be 140 kJ mol^{-1}. This is much lower than the values reported in the literature [10–13,18,23]. In paragraph 3, it was shown that the oxygen pulse experiments were performed at high coverage. Repulsive interactions and surface reconstruction at this high coverage could be the

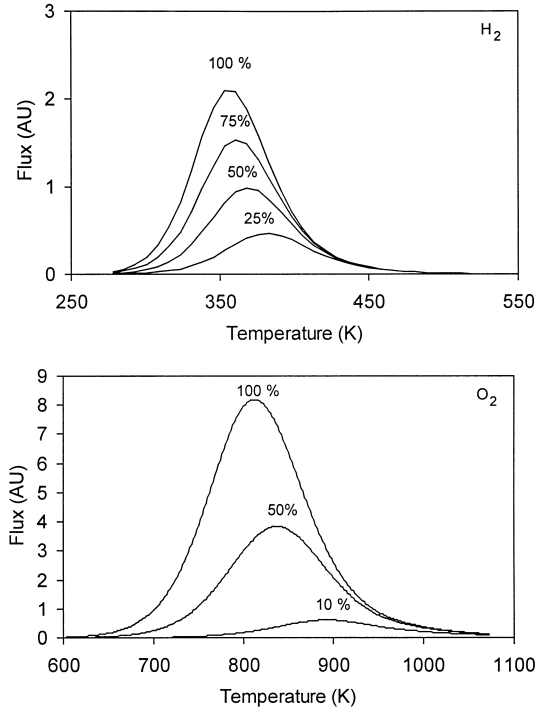

Fig. 6. Simulated TPD responses of hydrogen and oxygen at different initial coverages.

cause of the low activation energy for oxygen desorption [11,21,22]. Another possible cause are strong interactions between the support γ-Al_2O_3 and the Rh. Wang and Yeh [23] did not detect a significant influence of the Rh particle size on the heat of adsorption of oxygen on α-Al_2O_3 supported Rh catalysts, but it is well known that γ-Al_2O_3 catalysts show much stronger interactions with Rh particles than α-Al_2O_3.

6. Conclusion

The sorption of hydrogen and oxygen on a Rh/γ-Al_2O_3 catalyst with low Rh loading was studied by means of single pulse experiments in a TAP reactor and by means of simulation and regression of the pulse responses. A second-order dependence of the adsorption rate and the desorption rate with respect to the concentration of gas phase hydrogen and the concentration of adsorbed hydrogen leads to an excellent simulation of the hydrogen pulse responses. The kinetics agree with literature data. The model for the adsorption of oxygen consists of reversible dissociative oxygen adsorption and of exchange of adsorbed oxygen between a second adsorption state. The activation energy of oxygen desorption is lower than the values reported in the literature at low surface coverage. This is probably caused by repulsive interactions or surface reconstruction at high coverage.

7. Symbols and notations

Roman symbols

C_g	Gas phase concentration, mol m_g^{-3}
C_{H_2}	Gas phase concentration of hydrogen, mol m_g^{-3}
C^i	Initial conditions at iteration i
C_{O_2}	Gas phase concentration of oxygen, mol m_g^{-3}
C_s	Concentration of surface components, mol kg_c^{-1}
C_t	Concentration of sorption sites, mol kg_c^{-1}
D_c, D_i	Knudsen diffusivities in the catalyst and inert bed, $m_g^3\ m_r^{-1}\ s^{-1}$
E_d	Activation energy of the desorption rate coefficient, kJ mol^{-1}
E_{12}, E_{21}	Activation energies of the exchange rate r_{12} and r_{21}, kJ mol^{-1}
F_{in}	Flux at the inlet of the reactor, mol s^{-1}
k_a	Adsorption rate coefficient, $m_r^3\ kg_c^{-1}\ s^{-1}$
k_d	Desorption rate coefficient, mol $kg_c^{-1}\ s^{-1}$
k_{12}, k_{21}	Exchange rate coefficients between the adsorbed oxygen species, mol $kg_c^{-1}\ s^{-1}$
l	Active site
L_c	Depth of the catalyst bed, m_r
L_e	Depth of the exit bed, m_r
L_i	Depth of the inlet bed, m_r
M	Molecular weight, kg mol^{-1}
N_o	Pulse size, mol
q	Fraction of the surface in the reactor taken by active phase
R	Universal gas constant, J $mol^{-1}\ K^{-1}$
r_a	Adsorption rate, mol $kg_c^{-1}\ s^{-1}$
r_d	Desorption rate, mol $kg_c^{-1}\ s^{-1}$
$R_{v,g}$, $R_{v,s}$	Rates of formation of the gas phase and surface components, mol $kg_c^{-1}\ s^{-1}$
r_{12}, r_{21}	Exchange rates between the adsorbed oxygen species, mol $kg_c^{-1}\ s^{-1}$
S	Cross-section of the reactor, m_r^2
s_o	Sticking probability on an active site
t	Time, s
T	Temperature, K
u	Mean velocity of the gas phase molecules, $m_r\ s^{-1}$

V_o	Volume of the inlet section of the reactor, m_r^3
z	Axial position in the reactor, m_r
Z	Collision frequency, mol s^{-1} m_r^{-3}

Greek symbols

Δt	Pulse period, s
ε_c, ε_i	Void fractions of the catalyst and inert packing, m_g^3 m_r^{-3}
Λ	Mean free path in the catalyst bed, m_r
ρ_B	Bulk density of the catalyst bed, kg_c m_r^{-3}
θ_H	Surface coverage of adsorbed hydrogen
θ_O, θ_{O^*}	Surface coverage of chemisorbed oxygen

Acknowledgements

Olivier Dewaele acknowledges the Fund for Scientific Research-Flanders for a Research Assistant Fellowship. Dezheng Wang is grateful to the Fund for Scientific Research- Flanders for a fellowship in their Belgian–Sino cooperation program, and the Dalian Institute of Chemical Physics and the Chinese Academy of Sciences for granting a leave of absence. Glenn Creten is acknowledged for valuable discussions and Tom de Gres for help during experiments.

References

[1] S.H. Oh, P.J. Michtell, R.M. Siewert, J. Catal. 132 (1991) 287.
[2] J.R. Rostrup-Nielsen, J.-H. Bak Hansen, J. Catal. 144 (1993) 38.
[3] B.A. Sexton, G.A. Somorjai, J. Catal. 46 (1977) 167.
[4] S. Fuentes, F. Figueras, J. Catal. 61 (1980) 443.
[5] D.J.C. Yates, P.A. Thiel, W.H. Weinberg, Surf. Sci. 82 (1979) 45.
[6] D.J.C. Yates, P.A. Thiel, W.H. Weinberg, Surf. Sci. 84 (1979) 427.
[7] V.J. Mimeault, R.S. Hansen, J. Chem. Phys. 45 (1966) 2240.
[8] V.V. Gorodetskii, B.E. Nieuwenhuys, W.M.H. Sachtler, G.K. Boreskov, Appl. Surf. Sci. 7 (1981) 355.
[9] D.G. Castner, B.A. Sexton, G.A. Somorjai, Surf. Sci. 71 (1978) 519.
[10] G. Comelli, V.R. Dhanak, M. Kiskinova, N. Pangher, G. Paolucci, K.C. Prince, R. Rosei, Surf. Sci. 269/270 (1992) 360.
[11] T.W. Root, L.D. Schmidt, G.B. Fisher, Surf. Sci. 134 (1983) 30.
[12] D.N. Belton, G.B. Fisher, C.L. DiMaggio, Surf. Sci. 233 (1990) 12.
[13] P.A. Thiel, J.T. Yates Jr., W.H. Weinberg, Surf. Sci. 82 (1979) 22.
[14] S.-H. Chou, C.-T. Yeh, J. Chem. Soc., Faraday Trans. 92 (1996) 1409.
[15] A.M. Efstathiou, C.O. Bennett, J. Catal. 124 (1990) 116.
[16] M.P. Zum Mallen, W.R. Williams, L.D. Schmidt, J. Phys. Chem. 97 (1993) 625.
[17] D.F. Padowitz, S.J. Sibener, Surf. Sci. 254 (1991) 125.
[18] G. Comelli, V.R. Dhanak, M. Kiskinova, N. Pangher, G. Paolucci, K.C. Prince, R. Rosei, Surf. Sci. 260 (1992) 7.
[19] Y. Kim, S.-K. Shi, J.M. White, J. Catal. 61 (1980) 374.
[20] G.L. Kellog, J. Catal. 92 (1985) 167.
[21] C. Voss, N. Kruse, Surf. Sci. 409 (1998) 252.
[22] D. Alfè, S. de Goroncoli, S. Baroni, Surf. Sci. 410 (1998) 151.
[23] C.-B. Wang, C.-T. Yeh, J. Mol. Catal. A 120 (1997) 179.
[24] V. Nehasil, I. Stara, V. Matolin, Surf. Sci. 377 (1997) 813.
[25] E.S. Putna, J.M. Vohs, R.J. Gorte, Surf. Sci. 391 (1997) L1178.
[26] J.T. Gleaves, J.R. Ebner, T.C. Kuechler, Catal. Rev. Sci. Eng. 30 (1989) 43.
[27] B. Zou, M.P. Dudukovic, P.L. Mills, Chem. Eng. Sci. 48 (1993) 2345.
[28] W.C. Conner, G.M. Pajonk, S.J. Teichner, Adv. Catal. 34 (1987) 1.
[29] S.H. Oh, J.E. Carpenter, J. Catal. 80 (1983) 472.
[30] Y. Kim, S.-K. Shi, J.M. White, J. Catal. 61 (1980) 374.